Am J Physiol Lung Cell Mol Physiol 292: L40–L53, 2007.
First published August 4, 2006; doi:10.1152/ajplung.00425.2005.

Modeling the effect of stretch and plasma membrane tension on Na^+-K^+-ATPase activity in alveolar epithelial cells

Jacob L. Fisher[1] and Susan S. Margulies[1,2]

[1]*Department of Bioengineering, and* [2]*Institute for Medicine and Engineering, University of Pennsylvania, Philadelphia, Pennsylvania*

Submitted 4 October 2005; accepted in final form 24 July 2006

Fisher, Jacob L., and Susan S. Margulies. Modeling the effect of stretch and plasma membrane tension on Na^+-K^+-ATPase activity in alveolar epithelial cells. *Am J Physiol Lung Cell Mol Physiol* 292: L40–L53, 2007. First published August 4, 2006; doi:10.1152/ajplung.00425.2005.—While a number of whole cell mechanical models have been proposed, few, if any, have focused on the relationship among plasma membrane tension, plasma membrane unfolding, and plasma membrane expansion and relaxation via lipid insertion. The goal of this communication is to develop such a model to better understand how plasma membrane tension, which we propose stimulates Na^+-K^+-ATPase activity but possibly also causes cell injury, may be generated in alveolar epithelial cells during mechanical ventilation. Assuming basic relationships between plasma membrane unfolding and tension and lipid insertion as the result of tension, we have captured plasma membrane mechanical responses observed in alveolar epithelial cells: fast deformation during fast cyclic stretch, slower, time-dependent deformation via lipid insertion during tonic stretch, and cell recovery after release from stretch. The model estimates plasma membrane tension and predicts Na^+-K^+-ATPase activation for a specified cell deformation time course. Model parameters were fit to plasma membrane tension, whole cell capacitance, and plasma membrane area data collected from the literature for osmotically swollen and shrunken cells. Predictions of membrane tension and stretch-stimulated Na^+-K^+-ATPase activity were validated with measurements from previous studies. As a proof of concept, we demonstrate experimentally that tonic stretch and consequent plasma membrane recruitment can be exploited to condition cells against subsequent cyclic stretch and hence mitigate stretch-induced responses, including stretch-induced cell death and stretch-induced modulation of Na^+-K^+-ATPase activity. Finally, the model was exercised to evaluate plasma membrane tension and potential Na^+-K^+-ATPase stimulation for an assortment of traditional and novel ventilation techniques.

ventilator-induced lung injury; lipid trafficking; edema recovery

INVESTIGATORS HAVE FOUND alveolar epithelial stretch magnitude to be related to cell injury in vitro (55, 56) and tidal volume to be related to ventilator-induced lung injury (VILI) in animal models (12–15). Studies have revealed that the frequency of epithelial stretch or ventilation can also be an important factor in cell injury (56, 60). The model developed in this study examines how combinations of amplitude and frequency in ventilation procedures affect Na^+-K^+-ATPase activity via hypothesized pathways including alveolar epithelial cell plasma membrane tension and stretch-activated channel (SAC) stimulation.

To date, numerous models have been proposed to describe cellular mechanical behavior, from early continuum viscoelastic representations for erythrocytes and leukocytes (11, 27, 65) to more sophisticated variations that modeled cell membrane and the cortical cytoskeleton as a cortical shell with prestress (9, 11, 37), membrane viscosity (63), and/or a bending rigidity (64), and the cytoplasm as a Newtonian (63), Maxwell (10, 11), or power-law (51, 52) fluid. Other investigators have proposed models that focus on mechanical contributions of discrete cellular elements, such as tensegrity (4, 28, 47), percolation (20), and the cellular solid (42) models. None of these models, however, has focused on the plasma membrane as a separate cellular component. Generally, the overall deformation of a cell is determined by the cytoskeleton, cortical cytoskeleton, or the cytoplasm rather than mechanical deformation of the plasma membrane (26, 27, 65). Thus plasma membrane tension is usually considered secondary to mechanical responses of other cellular components. In most models, the plasma membrane is lumped with the cortical cytoskeleton. But unlike the cortical cytoskeleton, which is often assumed to be an elastic shell, the plasma membrane is flaccid and can respond to deformation by unfolding a ruffled surface (31, 57, 58) or by inserting lipids from a reservoir of additional plasma membrane material (39). In this study, we develop a model for the unique tension-area relationship of the plasma membrane to gain insight into the etiology of stretch-induced functional responses we have measured previously (18, 19). Namely, we have demonstrated that mechanogated channels in the plasma membrane transduce signals for stimulating cell responses, such as trafficking of Na^+-K^+-ATPase to the cell membrane and consequently enhancing Na^+-K^+-ATPase activity (19). However, high membrane tension can rupture a cell membrane, leading to cell death. For these reasons, a model specifically predicting alveolar epithelial cell plasma membrane tension in response to cell stretch could be a helpful tool in evaluating and selecting ventilation strategies that promote positive cell responses.

Research over the past decade has generated fundamental data on plasma membrane mechanical behavior that inform the plasma membrane model developed here. Investigators have reported lipid insertion as a protective mechanism against high membrane tension (7, 34, 61), similar to behavior we have previously reported for alveolar epithelial cells undergoing tonic stretch (18). Investigators have also pointed to ruffled plasma membranes as protection against membrane lysis in case of rapid deformation (31, 57). Because alveolar epithelial cells tolerate cyclic stretch in vivo and in vitro at much faster rates than lipid recruitment occurs, we hypothesize that alveolar epithelial cell plasma membrane expansion probably occurs as a combination of two phenomena, rapid cell surface unfolding and slower lipid insertion.

Address for reprint requests and other correspondence: S. Margulies, Dept. of Bioengineering, Univ. of Pennsylvania, 3320 Smith Walk, Philadelphia, PA 19104-6392 (e-mail: margulie@seas.upenn.edu).

The costs of publication of this article were defrayed in part by the payment of page charges. The article must therefore be hereby marked "*advertisement*" in accordance with 18 U.S.C. Section 1734 solely to indicate this fact.

In this study, we have created a theoretical model that incorporates the contributions of membrane unfolding and lipid insertion to relieve plasma membrane tension. We predict Na^+-K^+-ATPase activity in response to modeled membrane tension output based on biophysical channel opening theory, and we compare predictions with Na^+-K^+-ATPase activity measurements we have reported previously (19). As a proof of concept experiment, alveolar epithelial cells were stretched statically to allow plasma membrane expansion and then stretched cyclically. A "conditioning" effect, predicted by the model, was measured through changes in Na^+-K^+-ATPase activity. Conditioning was also observed in cell mortality and basolateral membrane (BLM) content of Na^+-K^+-ATPase α_1-subunit. Finally, the model was exercised to predict alveolar epithelial membrane tension and relative Na^+-K^+-ATPase stimulation in cells subjected to conventional and innovative ventilation strategies.

Model development. The objective of this modeling effort is to predict increases in Na^+-K^+-ATPase activity for given alveolar epithelial deformation patterns derived from clinically relevant mechanical ventilation maneuvers. With these predictions we will evaluate different ventilation strategies in terms of their effectiveness in stimulating a desirable increase in Na^+-K^+-ATPase activity. A flowchart of this overall scheme is shown in Fig. 1. Black arrows indicate previously established discoveries, namely that cyclic stretch acts through SACs to induce greater Na^+-K^+-ATPase activity and does so by increasing the number of Na^+-K^+-ATPases in the BLM (19), and that tonic stretch stimulates lipid insertion into the plasma membrane (18). The gray arrow in Fig. 1 represents a biophysics theory, which states that SAC opening probability is described by a Boltzmann distribution dependent on tension over the SAC (22, 24, 29, 30, 32, 41). The dashed black arrows represent relationships between stretch and plasma membrane tension, including a negative feedback mechanism created by tension-reducing lipid insertion, all of which we wish to predict with a mathematical model fit to data derived from the appropriate literature. Finally, white arrows in Fig. 1 represent the interrelationship between stretch, plasma membrane tension, and lipid trafficking, which is not only influenced by tension but also serves as negative feedback by reducing tension. These white arrow relationships will be provided by the model developed here. Also, solid arrows show direct relationships, whereas broken arrows indicate indirect but observed relationships between stimuli and responses. The following subsections describe model conceptualization and fundamental assumptions, model formulation, and parameter fitting.

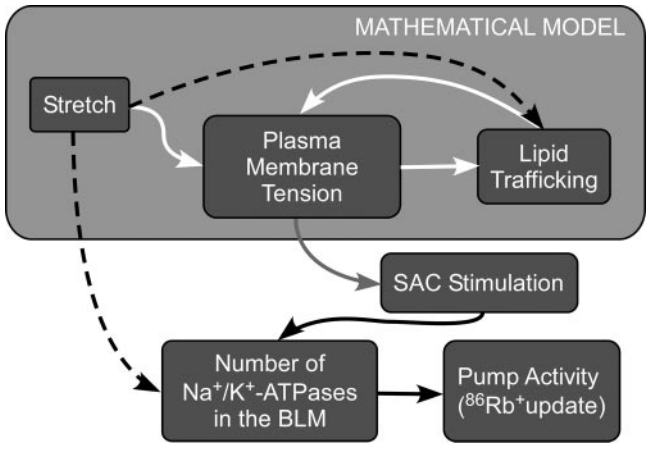

Fig. 1. Model flowchart. The goal of this study is to combine several previously reported cellular responses to stretch and combine them into a comprehensive model that predicts Na^+-K^+-ATPase stimulation for any stretch pattern according to the relationships shown above. Black arrows represent previously reported alveolar epithelial cell behavior. The gray arrow represents biophysics theory of stretch-activated channel opening in response to tension, discussed in this study. Finally, white arrows represent the interrelationship between stretch, plasma membrane tension, and lipid trafficking, which is not only influenced by tension, but also serves as negative feedback by reducing tension. These relationships, in white text, will be provided by the mathematical model developed here. Also, solid arrows show direct relationships, whereas broken arrows indicate indirect but reported relationships between stimuli and responses. SAC, stretch-activated channel.

Model conceptualization. The first premise behind our mathematical model is that equibiaxially stretched alveolar epithelial cells initially respond by unfolding their cell surface. Because the undisturbed plasma membrane generally has a ruffled shape provided by an underlying cytoskeletal scaffolding, this unfolding requires work and results in a corresponding tension and elastic strain energy in the plasma membrane. Our second premise posits that this membrane tension stimulates SACs and lipid insertion in the plasma membrane, as suggested by SAC stimulation (19) and lipid insertion (17). Specifically, we assume that SACs respond instantly to tension, whereas we require that lipid insertion occur more slowly, as shown by lipid insertion observed during tonic stretch (18, 23). Based on observations of lipid resorption in flaccid cells (7, 18, 33, 61), we also propose that lipid resorption occurs when the cell shrinks or is released after stretch and an excess of flaccid membrane exists. This insertion and resorption of lipid will reduce and restore membrane tension, respectively.

The paucity of quantitative empirical knowledge regarding the relationship between plasma membrane stretch and tension, or between tension and either lipid insertion or resorption, necessitates several assumptions. First, we have assumed a simple Hookian elastic relationship between plasma membrane unfolding (area deformation) and plasma membrane tension. Second, we have assumed that the rate of lipid insertion is proportional to plasma membrane tension; that is, the higher membrane tension, the faster additional lipid inserts into the membrane. Finally, we have assumed that if the cell shrinks or is forcibly shrunken by imposed deformation, the cell resorbs excess membrane at a rate proportional to the amount of excess.

These assumptions can be formulated into mathematical relationships. The assumed Hookian relationship between plasma membrane surface area increase due to unfolding, $A - A_0$, and tension, T_{BI}, is similar to that of a spring. However, unlike a typical spring, under tension the plasma membrane has the capacity to add more "spring material" via lipid insertion, increasing its neutral (zero tension) area and reducing tension. Hence we use A^* to represent a variable neutral or gauge area, which expands via lipid insertion. Plasma membrane tension, T_{BI}, is governed by the relationship:

$$T_{BI} = K_{BI}\left(\frac{A - A^*}{A_0}\right) = K_{BI}(\alpha - \alpha^*) \qquad (1)$$

where K_{BI} is an area elastic modulus, A is cell surface area, A_0

is initial cell surface area, α is a relative area strain, and α^* is defined as

$$\left(\frac{A^* - A_0}{A_0}\right),$$

the proportional increase in the neutral area or neutral strain.

We also assumed stretch stimulates lipid insertion at a rate proportional to the stretch-induced tension so that the neutral strain, α^*, can increase as follows:

$$\eta_i \dot{\alpha}^* = T_{BI},$$

where η_i is a lipid insertion modulus and

$$\dot{\alpha}^* = \frac{d\alpha^*}{dt} \quad (2)$$

Combining *Eqs. 1* and *2* yields

$$\eta_i \dot{T}_{BI} + K_{BI} T_{BI} = \eta_i K_{BI} \dot{\alpha} \quad (3)$$

The model described by *Eq. 3*, however, is incomplete because it predicts that lipid insertion can produce complete membrane relaxation, allowing tension to diminish to zero under constant deformation. Contrary to this prediction, investigators have found that tension did relax partially after increasing with deformation in osmotically swollen cells, but it did not disappear completely (7, 8). Furthermore, they found that a released cell, even after lipids have been added, still recovered its initial shape and size (6, 7). To incorporate these additional characteristics we add a second elastic unfolding element, which we will designate Branch II, in parallel with the existing model in *Eq. 3*, which we will call Branch I. Like Branch I, which was just derived, Branch II represents a spring-like Hookian relationship between tension and the cell surface area deformation produced by unfolding, but, unlike Branch I, Branch II is not affected by lipid insertion. Thus the deformation for the second elastic element is:

$$T_{BII} = K_{BII}\left(\frac{A - A_0}{A_0}\right) = K_{BII}\alpha \quad (4)$$

where the reference area for determining the amount of deformation is initial surface area A_0 instead of neutral area A^*. The total plasma membrane tension, T, is the sum of $T_{BI} + T_{BII}$.

In sum we represent the plasma membrane as a two-branch elastic solid (Fig. 2). The elastic element in Branch I can take on additional material when it is under tension, resulting in tension relaxation as A^* increases beyond A_0. In contrast, the elastic solid in Branch II does not relax but instead maintains a tension proportional to area deformation relative to the initial neutral state, A_0. This reference to A_0 as a baseline in Branch II supplies a persistent tension in the whole model, even if lipid insertion and complete tension relaxation occur in Branch I, and thus provides the recoil required for the released cell to recover its initial shape.

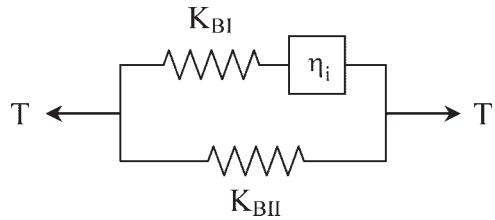

Fig. 2. Three-element mechanical model. The plasma membrane model is composed of a 2 Hookian springs with elastic moduli K_{BI} and K_{BII}, representing plasma membrane resistance to unfolding. Unlike a standard spring, the upper arm, Branch I, has the capacity to supplement itself with additional material at a rate, η_i, proportional to tension. This lipid insertion increases the neutral area of Branch I, relaxing tension, T.

Released from stretch, the cell shrinks naturally or is forced to shrink by elastic contraction of adjacent materials (in vitro) or tissue (in vivo). As the cell shrinks, tension in Branch II remains positive as long as surface area A remains larger than the initial area, A_0. In contrast, due to the lipid inserted to the plasma membrane, Branch I possesses an excess of plasma membrane when the imposed shrunken area A is less than A^*. Because the plasma membrane has a negligible bending stiffness (25), it bears almost no compression before buckling and bunching into ruffles. Thus tension in Branch I becomes zero when $A = A^*$ and remains zero as long as $A < A^*$. The buckling of excess membrane beyond "normal" membrane folding is energetically unfavorable and leads to membrane resorption, as observed experimentally (5–7, 34). Earlier, our third assumption proposed that the rate of this lipid resorption is proportional to the amount of excess membrane; mathematically stated:

$$\beta \dot{\alpha}^* = (\alpha - \alpha^*) \quad (5)$$

where β is a strictly positive absorption modulus. Hence, when $\alpha < \alpha^*$ and excess lipid exists during imposed shrinking, $\dot{\alpha}^* < 0$, indicating plasma membrane resorption.

Model constitutive equations. The overall constitutive equations for the model proposed above are derived from the individual properties of its component elements. Total tension, T, is the sum of tensions in Branch I and Branch II. Differentiating over the total deformation and substituting *Eqs. 1* and *2* yield the governing equation during cell expansion:

$$T + a\dot{T} = b\alpha + c\dot{\alpha} \quad (6)$$

where

$$a = \frac{\eta_i}{K_{BI}}, \quad b = K_{BII}, \quad \text{and} \quad c = \eta_i\left(1 + \frac{K_{BII}}{K_{BI}}\right). \quad (7)$$

When the cell shrinks ($\alpha < \alpha^*$), tension disappears in Branch I. Unlike lipid insertion rate, which is defined as proportional to tension, lipid resorption rate is assumed proportional to the amount of excess membrane, $\alpha^* - \alpha$, so we combine *Eqs. 4* and *5* to derive the governing equation during cell shrinkage:

$$P + \hat{a}\dot{P} = \hat{b}\alpha + \hat{c}\dot{\alpha} \quad \text{where} \quad P = T + \gamma(\alpha - \alpha^*) \quad (8)$$

where γ is simply a dimensional conversion scalar with units of tension, and the coefficients $\hat{a}$, $\hat{b}$, and $\hat{c}$ are combinations of the moduli K_{BII}, β, and γ.

$$\hat{a} = \beta, \quad \hat{b} = K_{BII}, \quad \text{and} \quad \hat{c} = \beta(\gamma + K_{BII}). \quad (9)$$

Importantly, we note that at the point where lipid insertion stops and lipid resorption begins and vice versa, there is no excess plasma membrane, tension in Branch I is zero, and $P = T$. A full derivation of this model with greater detail has been published elsewhere (16).

Parameter fitting. Because plasma membrane tension, cell capacitance, and cell size measurements all require probing or

imaging at a microscopic level, it is presently impossible to stretch cells physically via conventional techniques and simultaneously make microscopic measurements. Thus we relied on data from two similar osmotic cell-swelling and -shrinking studies from Dai et al. (7, 8) to fit the relevant model parameters. In these experiments using custom-made apparatus, the medium surrounding a continuously probed cell was carefully changed, first to a 50% hypotonic solution to cause osmotic swelling, which increased plasma membrane tension and promoted creep, and then to an isotonic medium to relieve osmotic pressure and membrane tension and to allow the cell to shrink. In the more recent communication (7) the investigators swelled and shrunk cells osmotically and recorded the following: plasma membrane tension measured via force in a plasma membrane tether pulled from the cell using a bead and optical trap; whole cell capacitance measured via a micropipette-perforated patch technique; and total cell volume, calculated through a cell diameter measurement, roughly assuming the cell to be spherical. In the earlier communication (8), the investigators had only swelled the cells and had only recorded plasma membrane tension and cell volume, but with greater temporal resolution than in the recent study. We have used data from both studies to fit the parameters in *Eqs. 8A* and *11*. In cases where plasma membrane tension was reported as tether force, F, force was converted to cell membrane tension, T, using a relationship derived by the authors (45):

$$F = 2\pi\sqrt{2BT}, \qquad (10)$$

where B, the membrane bending stiffness, is 2.7×10^{-19} N × m (25).

We acknowledge at this point that the data used for model parameter fitting were collected from neuronal cells rather than alveolar epithelial cells. Nevertheless, many basic characteristics such as overall change in cell capacitance and cell size under a given load and relaxation constants were similar between the neuronal cells used for parameter fitting and data obtained by our lab and others for alveolar epithelial cells (6, 7, 57, 58).

Parameter values found to produce a least squares fit between model-generated output and observed data are listed in Table 1.

EXPERIMENTAL METHODS

For use in proof-of-concept conditioning experiments, alveolar type 2 (AT2) cells were isolated from male, Sprague-Dawley rats (Charles River, Wilmington, MA) (55) and cultured using established, previously described methods (18, 19, 55). AT2 cells were then seeded for confluence at 1×10^6 cells/cm^2. To determine whether lipid trafficking during static stretch has any conditioning effect on cells, 2-day cells were tonically prestretched before being stretched cyclically in a custom-made stretching device capable of imposing uniform, equibiaxial two-dimensional strain (16, 55). Preconditioning was performed by stretching cells tonically for 10 min to a prescribed change in substrate surface area (ΔSA). At the end of this period, any preconditioned control wells not slated for stretch would be quickly removed from the device (while others remained statically stretched). Then the motor of the stretching device was switched on, beginning cyclic stretch with a falling wave from the peak stretched position. Within the first minute of cyclic stretch, stretched but unconditioned wells would be fastened into place while the device was in operation. Thus preconditioned wells were held in the stretch position until cyclic stretch began to eliminate the possibility of excess membrane endocytosis during well changes. Cyclic stretch was carried out at either 25% or 37% ΔSA for 60 min at 15 cycles/min. After stretch, cell viability, Na^+-K^+-ATPase activity as measured by $^{86}Rb^+$ uptake, or Na^+-K^+-ATPase α_1-subunit content in the AT2 BLM were measured using published techniques (19).

Viability, Na^+-K^+-ATPase activity, and Na^+-K^+-ATPase trafficking data from were analyzed using previously described methods (16, 19). Differences in viability were assessed using two-way ANOVA over treatment (preconditioned and unconditioned) and over three isolations at each stretch magnitude. Na^+-K^+-ATPase activity in conditioned cells was assessed relative to unstretched controls. To compare conditioned cell results and previous results for stretch without conditioning, data were normalized by internal controls and compared by two-way ANOVA over treatment (conditioned and unconditioned) and over four isolations in each treatment. Na^+-K^+-ATPase α_1-subunit blot densities were compared using paired *t*-tests ($P \leq 0.01$ for significance) among cells stretched without conditioning, cells stretched with conditioning, and unstretched cells. Tukey's procedure for honestly significant differences was used to correct for multiple comparisons.

Table 1. *Model parameters determined by data fitting*

Swell		Shrink	
a	3.79 s	$\hat{a}$	3.58 s
b	0.0289 dyn/cm	$\hat{b}$	0.0289 dyn/cm
c	0.570 dyn-s/cm	$\hat{c}$	3.68 dyn-s/cm
K_{BII}	0.0289 dyn/cm	K_{BII}	0.0289 dyn/cm
K_{BI}	0.121 dyn/cm	β	3.58 s
η_i	0.460 dyn-s/cm		

K_{BI} and K_{BII}, area elastic moduli; η_i, lipid insertion modulus; β, strictly positive absorption modulus; coefficients *a, b,* and *c*, combinations of the moduli K_{BI} and K_{BII} and η_i, for membrane swelling; coefficients $\hat{a}$, $\hat{b}$, and $\hat{c}$, combinations of the modulus K_{BII}, β, and γ.

RESULTS

Tonic-stretch preconditioning attenuates cyclic stretch responses. Preconditioning alveolar epithelial cells with tonic stretch significantly reduced their response to subsequent cyclic stretch. In viability studies, cells stretched at 25% ΔSA saw a significant decrease in cell death from 15.3 ± 4.2% to 5.6 ± 1.9% with 10 min of tonic prestretch. Results were similar at 37% ΔSA, at which the mortality rate decreased from 14.2 ± 1.1% in unconditioned cells to 6.4 ± 0.8% in preconditioned cells (Fig. 3). At both magnitudes, analysis of variance detected significant differences between conditioned and unconditioned treatments ($P < 0.001$). It should be noted that preconditioning had no negative effect on cell adherence or cell density.

Similarly, tonic-stretch conditioning resulted in attenuated Na^+-K^+-ATPase activity. Cells tonically prestretched for 10 min at 25% ΔSA and then cyclically stretched at 15 cycles/min for 1 h at the same magnitude increased Na^+-K^+-ATPase activity by only 53% (1.53 ± 0.10) over unstretched controls (1.00 ± 0.06) in contrast to 136% increase for cyclically stretched cells (2.36 ± 0.25 for stretched cells vs. 1.00 ± 0.20 for separate, unstretched controls; Fig. 4). Western blot density of BLM Na^+-K^+-ATPase α_1-subunit in preconditioned cells also rose significantly (1.79 ± 0.19 intensity units, normalized by controls) over unstretched controls (1.00 ± 0.11), but significantly less than in stretched cells that had not been conditioned with tonic stretch beforehand (2.44 ± 0.21; Fig. 5).

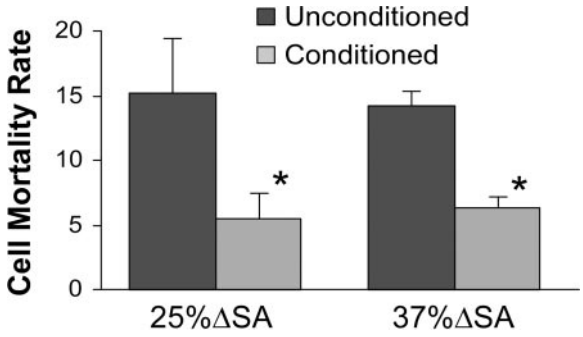

Fig. 3. Effect of tonic-stretch conditioning on cell viability. Stretching cells tonically for 10 min before stretching them cyclically for 1 h at the same magnitude significantly reduced cell viability relative to cells stretched cyclically without conditioning. Bars represent means ± SE; $n = 18$. An asterisk (*) over a bar represents significant difference from control. Significance ($P < 0.05$) was determined by 2-way ANOVA between conditioned and unconditioned cells over 3 isolations at each stretch magnitude. Viability in all controls was >99% and is not shown. ΔSA, change in surface area.

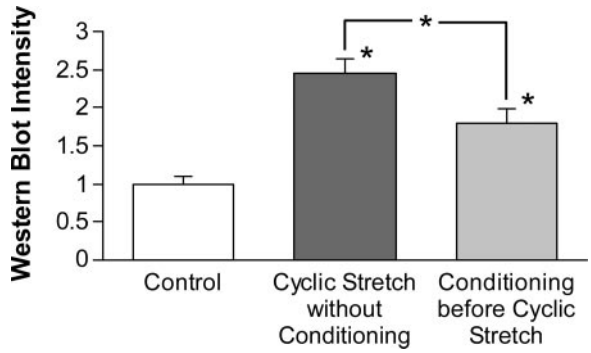

Fig. 5. Effect of tonic-stretch conditioning on Na^+-K^+-ATPase trafficking. Stretching cells tonically for 10 min before stretching them cyclically for 1 h at 25% ΔSA significantly reduced Na^+-K^+-ATPase α_1-subunit levels in the BLM (1.79 ± 0.19) compared with α_1-subunit content in cells stretched without conditioning (2.44 ± 0.21). However, even in conditioned cells, α_1 content was significantly greater than in wholly unstretched control (1.00 ± 0.11). Bars represent means ± SE of Western blot intensity for Na^+-K^+-ATPase α_1-subunit, normalized to control values. Significance ($P < 0.01$) was determined by *t*-tests among the 3 groups using Tukey's procedure for honestly significant differences to correct for multiple comparisons. An asterisk (*) over a bar represents significant difference from control; an asterisk spanning groups shows significant difference between groups.

Model behavior. As a basic confirmation that the model can predict plasma membrane responses in agreement with our initial hypotheses, we inspected model predictions of plasma membrane tension, elastic deformation, and lipid insertion/resorption for a 25% ΔSA tonic-stretch input (Fig. 6), a 25% ΔSA cyclic stretch input (Fig. 7), and 25% ΔSA cyclic stretch after 10 min of tonic-stretch preconditioning (Fig. 8). In response to tonic deformation, the model predicted a peak membrane tension coinciding with the end of the initial stretch and associated with elastic deformation in both Branches I and II. As cell deformation was maintained, tension relaxed as lipid insertion occurred. Within 40 s, Branch I neutral area strain, α^*, increased to 25% ΔSA, the magnitude of the entire deformation, α (Fig. 6*C*). This baseline increase completely relaxed tension in Branch I so that the only tension in the total membrane was the tension in Branch II. At the end of the tonic-stretch experiment, stretch was released, and plasma membrane tension and total cell deformation both fell to zero, but excess plasma membrane accumulated at the cell surface as shown by the negative Branch I deformation (Fig. 6*D*). At this point, $\alpha^* > \alpha$, forcing lipid resorption, as indicated by the decreasing baseline area strain, α^* (Fig. 6*D*). As the cell resorbed excess lipid, α^* became zero, indicating no further excess membrane, reflected by the Branch I elastic deformation ascending from negative values (excess). Relaxation via lipid insertion during tonic stretch occurred more rapidly than resorption of additional lipid after release from tonic stretch (Fig. 6*D*). This same rate differential is illustrated in the fast rise and slow fall of capacitance in osmotically swollen and shrunken cells (7).

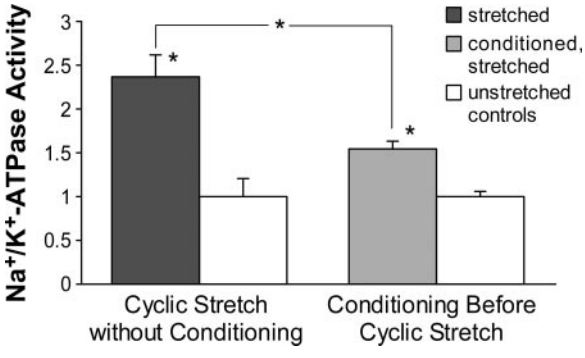

Fig. 4. Effect of tonic-stretch conditioning on Na^+-K^+-ATPase activity. Stretching cells tonically for 10 min before stretching them cyclically for 1 h at 25% ΔSA significantly lessened stretch-induced increases in Na^+-K^+-ATPase activity relative to activity in cells that were not conditioned before stretch. Bars represent means ± SE. Open bars indicate unstretched controls corresponding to each condition. Significance ($P < 0.05$) was determined by 2-way ANOVA between conditioned and unconditioned cells over 4 isolations at each stretch magnitude. An asterisk (*) over a bar represents significant difference from control; an asterisk spanning groups shows significant difference between groups.

In response to a cyclic stretch deformation (Fig. 7*A*), tension rose and fell cyclically (Fig. 7*B*), suggesting that lipid insertion did not take place as fast as deformations were imposed. However, the maximum and average tension imposed by a deformation did decrease over the first few cycles, implying that some relaxation occurred even during cyclic stretch. Comparing α^* between the first stretch cycle (Fig. 7*C*) and another later cycle after the tension wave achieved steady state (Fig. 7*D*) confirmed that lipid insertion had occurred. In the initial cycle α^* increased, but only to ≈9% ΔSA, not the full deformation of 25% ΔSA (Fig. 7*C*) because the rate of lipid insertion was slow relative to the deformation rate imposed by cyclic stretch. Thus the remainder of the deformation, $\alpha - \alpha^*$, took place elastically in Branch I, which added to the elastic tension of Branch II to generate the high tension predicted in the initial cycle. However, in a steady-state cycle, we find that the increased baseline α^* accounted for 15–20% ΔSA in a 25% ΔSA stretch (Fig. 7*D*). At this point, deformation in Branch I was largely negative, indicating an excess of plasma membrane through most of the cycle. Only at the peak of deformation did Branch I stretch elastically and contribute to membrane tension. However, because Branch I has a greater elastic modulus than Branch II, this small elastic Branch I deformation contributes significantly to overall membrane tension.

After 10 min of tonic-stretch preconditioning, the plasma membrane steady-state response to 25% ΔSA cyclic stretch was generally similar in form to the response to 25% ΔSA

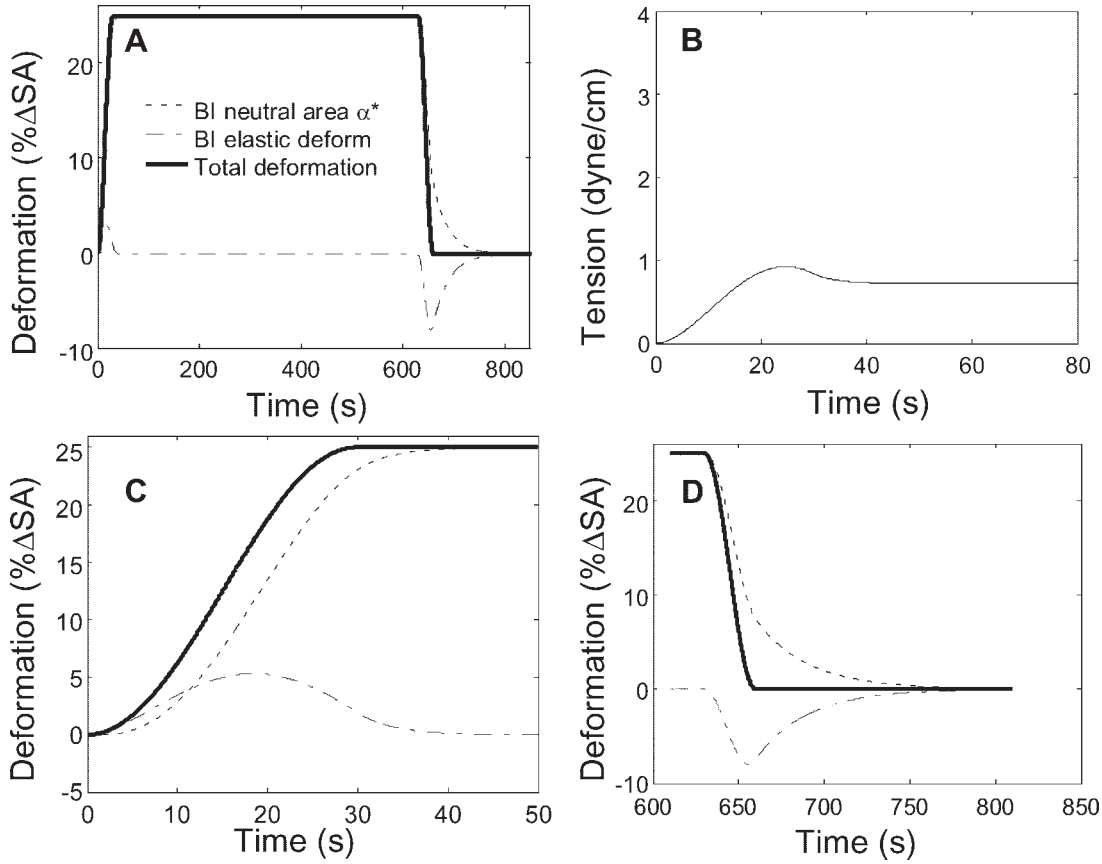

Fig. 6. Analysis of model output for tonic deformation. *A*: 25% ΔSA tonic input deformation, internal Branch I elastic deformation, and change in Branch I neutral area as a result of lipid insertion or resorption. *B*: the corresponding tension output, which initially rises and then relaxes. *C*: the mechanism of that relaxation, namely enlargement of the neutral area strain, α^*, via lipid insertion. As lipid inserts, the elastic deformation in Branch I wanes along with its corresponding tension. *D*: release from tonic stretch. Although deformation and tension both drop to zero at the end of stretch, the Branch I deformation actually becomes negative, representing an excess of inserted lipid. At this point, the relative baseline area strain (α^*) exceeds the area strain. As lipid is reabsorbed, α^* decreases, and the excess, shown as negative deformation, disappears. We note that lipid insertion in a tense membrane occurs faster than lipid reabsorption in a flaccid membrane.

cyclic stretch without preconditioning, but with slightly shifted magnitudes. As shown in Fig. 8*B*, cells began cyclic stretch with fully expanded Branch I neutral area, that is α^* was 25% ΔSA. Thus during the initial stretch cycles, Branch I deformation exploited the excess "slack" created by expanded α^* so that there was almost no elastic Branch I deformation. As cyclic stretch continued, plasma membrane resorption gradually occurred during the shrinking phase of each cycle until a steady state was reached. However, we note that steady-state cyclic plasma membrane deformation in preconditioned cells was different from that in unconditioned cells. Presumably due to faster lipid insertion relative to lipid resorption, the lipid inserted during tonic-stretch conditioning is never fully resorbed, creating a greater reserve of material and thus a greater neutral area strain, α^*, even after steady state is achieved. The result of this greater neutral area is less elastic deformation and thus lower tension in preconditioned cells.

In addition to the 25% ΔSA cyclic and 25% ΔSA tonic waves analyzed in detail above, tension output was generated for two additional deformation patterns: 12% ΔSA cyclic stretch and 12–25% ΔSA cyclic stretch (Fig. 9). In these additional tension oscillations, we observe the same pattern noted in cyclic stretch before: high tension peaks in the first few deformation cycles, but the wave diminishes and stabilizes in less than a minute, and continues with that form for the remainder of the 1-h stretch. On the whole, we find that the model produces quantitative results in agreement with previous qualitative observations: cyclic stretch produces higher tensions than tonic stretch; tonic stretch allows for lipid insertion and partial relaxation of tension, reducing a potential tension-induced stretch stimulus; and lipid resorption from a flaccid membrane occurs more rapidly than lipid insertion into a tense membrane. Making dynamic measurements of quantities such as plasma membrane tension or lipid insertion in a stretching cell is impossible with current techniques. Thus until dynamic measurement techniques are developed, this model provides estimates of plasma membrane tension and lipid insertion by extrapolating measurements made in slow osmotic swelling into the domain of fast dynamic deformation.

As a comparison of predicted model response to experimental measurements, we consider whether lipid turnover rates projected by the model are realistic. It is well known that a cell at rest regularly recycles plasma membrane to regulate surface protein expression, absorb nutrients, and secrete waste and physiologically important substances, such as surfactant in the case of alveolar epithelial type 2 cells. Previously, investigators have demonstrated that tonically stretched alveolar epithelial cells increase both exocytosis (59) and endocytosis (2), although overall

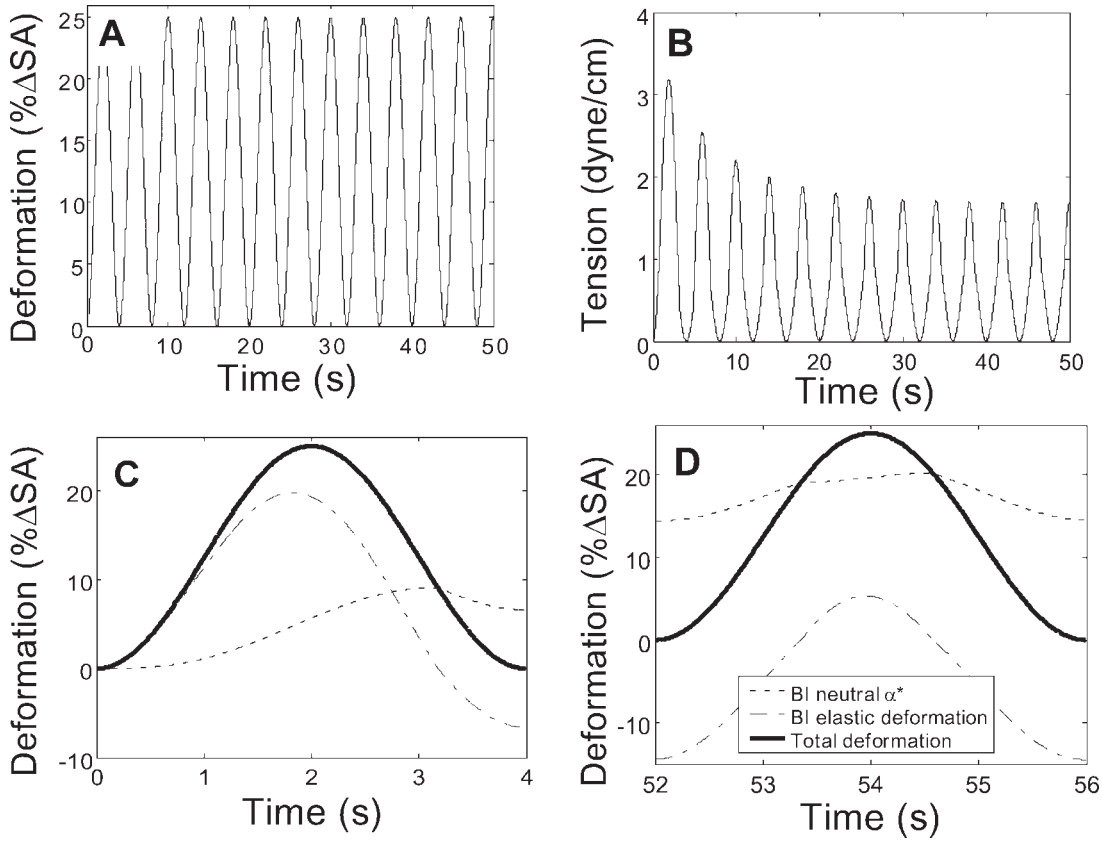

Fig. 7. Analysis of model output for cyclic deformation. *A* shows a 25% ΔSA cyclic deformation input, and *B* shows the similarly cyclic tension output. Initial tensions are high but, within 40 s, the tension output reaches a steady-state oscillation. The decrease in tension during the first 10 cycles is explained by the contrast in internal deformations between the first deformation cycle (*C*) and a deformation cycle after tension has stabilized (*D*). *C* shows that α^* enlarges via lipid insertion during the initial cycle but not nearly enough to relax Branch I sufficiently, leaving most of the deformation to tension-generating membrane unfolding. However, *D* indicates that after tension stabilizes, the baseline area (α^*) has expanded to between 15 and 20% ΔSA in a 25% ΔSA deformation. The negative values for Branch I deformation indicate an excess of membrane area during much of the cycle with elastic unfolding occurring only at the peak deformation.

turnover rates were not reported. In terms of mass balance, one can consider normal and stretch-induced lipid insertion as follows: $\dot{\alpha}^*$ = stretch-induced insertion rate − stretch-induced resorption rate + normal insertion rate − normal resorption rate.

In a resting cell, normal exocytosis and endocytosis rates are dynamically balanced so that plasma membrane surface area remains constant. With tonic stretch, insertion and resorption have both been shown to increase, although the rate of insertion clearly outpaces resorption as manifest in net plasma membrane expansion. In cell shrinking, the balance is reversed so that resorption dominates, resulting in net plasma membrane decrease. Whether insertion and resorption rates are both higher or both lower during tonic-stretch equilibrium is unknown, although investigators have demonstrated that pharmacologically induced endocytosis is hindered by increased plasma membrane tension in some cell types (6, 8), suggesting that normal exocytosis and endocytosis might both decrease. This could have important implications for AT2 cells, which regularly exocytose pulmonary surfactant. However, some studies suggest surfactant release employs so-called "kiss and run" exocytosis, in which a vesicle merges with plasma membrane, releases its contents from the cell, and closes again without fully integrating into the plasma membrane (43). In terms of whole cell lipid turnover, stretch-induced lipid insertion certainly calls on a cell's fullest lipid trafficking capacity. Hao and Maxfield (23) found that the half-time, $t_{1/2}$, for membrane turnover in resting CHO cells could be as short as 5–10 min. In previous studies, we found lipid trafficking to take place within 5 min (18); other investigators found deformation-induced lipid trafficking to occur within 90 s (59); and our model predicts a 25% ΔSA in 40 s. Thus in an extreme case, stretch-induced trafficking could be occurring at rates 7–8 times that of normal recycling of a resting cell. Although a potentially great demand on the cell, studies of lipid trafficking to repair plasma membrane stress failure suggest that such rates are not unreasonable (21, 48, 58).

Predicting Na^+-K^+-ATPase stimulation using tension to estimate SAC opening. Previously we demonstrated that stretch-induced SAC activation augments Na^+-K^+-ATPase activity (19). To relate plasma membrane tension to SAC activation, we employed a prevalent theory (29, 41, 49, 50) that the probability, P_o, of a SAC being open to ion traffic is determined by a Boltzmann probability distribution dependent on plasma membrane tension, T:

$$P_O = \frac{1}{1 + e^{\zeta(T - T_{1/2})}} \quad (11)$$

where $T_{1/2}$ is the tension at which the probability of SAC opening is 50% and ζ, sensitivity to tension, represents the

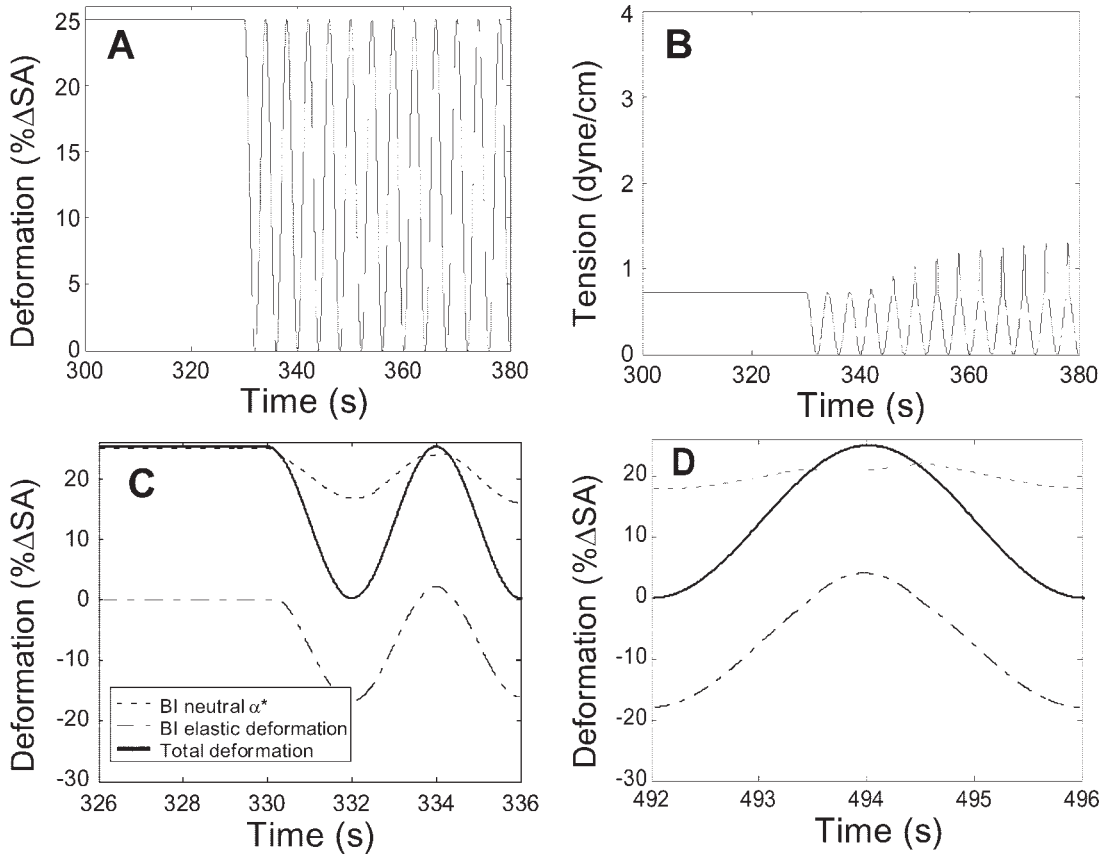

Fig. 8. Analysis of model output for 25% ΔSA cyclic deformation after tonic-stretch preconditioning. *A* shows a 25% ΔSA cyclic deformation input, and *B* shows the corresponding tension output after 10 min of tonic-stretch preconditioning. Initial cyclic tensions are low, but they gradually rise to steady-state oscillation. However, plasma membrane tension after preconditioning never achieves tension magnitude observed in unconditioned cyclic stretch (Fig. 7*B*). Internal deformations showing elastic deformation and changing neutral area are shown for the first deformation cycle after preconditioning in *C* and after tension has stabilized in *D*. *C* shows that the baseline area strain (α^*) starts fully expanded at 25% ΔSA. Thus in early cycles, elastic deformations are small, since the expanded neutral area material is not quickly resorbed and this slack is utilized for the initial cyclic deformations. However, *D* indicates that after the tension response stabilizes, the neutral area strain α^* has been resorbed somewhat. Comparing *D* with Fig. 6*D*, cyclic stretch without preconditioning, we notice that elastic deformations in Branch I are smaller in preconditioned membrane than in unconditioned membrane, accounting for the lower tensions. A lipid insertion rate faster than a resorption rate accounts for the persistent preconditioning effect.

tension change required to cause an *e*-fold increase in relative channel activity.

For our purposes, we performed parametric simulations over a range of values for ζ, and $T_{1/2}$ corresponding to a range of parameter values reported in the SAC classification literature (24, 29, 30, 41, 49, 50). Model-generated membrane tension was used to calculate a P_o "wave" via *Eq. 11* for five stretch patterns: 25% ΔSA tonic stretch, 12% ΔSA cyclic stretch, 25% ΔSA cyclic stretch, 12–25% ΔSA cyclic stretch, and 25% ΔSA tonic-stretch preconditioning followed by cyclic stretch. A cumulative SAC activity (CCA) was calculated by integrating P_o over 4 s, the duration of a typical deformation cycle at 15 cycles/min, in a part of the wave where steady-state tension output had been achieved:

$$\mathrm{CCA} = \int_{4s} P_O dt. \qquad (12)$$

Ultimately, parameters $T_{1/2}$ and ζ were adjusted to $T_{1/2} = 1.4$ dyn/cm and $\zeta = 8$ cm^2/erg to achieve the best linear correlation ($R^2 = 0.96$; Fig. 10) between previously published values of Na^+-K^+-ATPase activity increase (19) and CCA (based on an implicit assumption that Na^+-K^+-ATPase increases are directly proportional to SAC stimulation).

Matrix of model simulations. Once fit with data, the model was exercised to examine CCA and plasma membrane tension for several traditional and relatively novel mechanical ventilation strategies. Maneuvers selected for testing included ventilation with various tidal volumes, ventilation with several constant positive end-expiratory pressure (PEEP) magnitudes but the same peak tidal volume, ventilation with several constant PEEP magnitudes and the same tidal volume amplitude, ventilation with PEEP varying at 0.2 cycles/min, ventilation with tonic volume, and high frequency ventilation (HFV) (Fig. 11). Using clinically relevant values for ventilator tidal volume, PEEP, and frequency, deformation waves were created for each maneuver using, as necessary, a pressure-to-total lung capacity (TLC) conversion from West (62) and a TLC-to-% ΔSA conversion from Tschumperlin (53, 54). Deformation curves were used as inputs to the model to simulate plasma membrane tension curves, from which we extracted predicted tension and calculated CCA.

Deformation input categories. The first category contains cyclic oscillations at 15 cycles/min between an undeformed

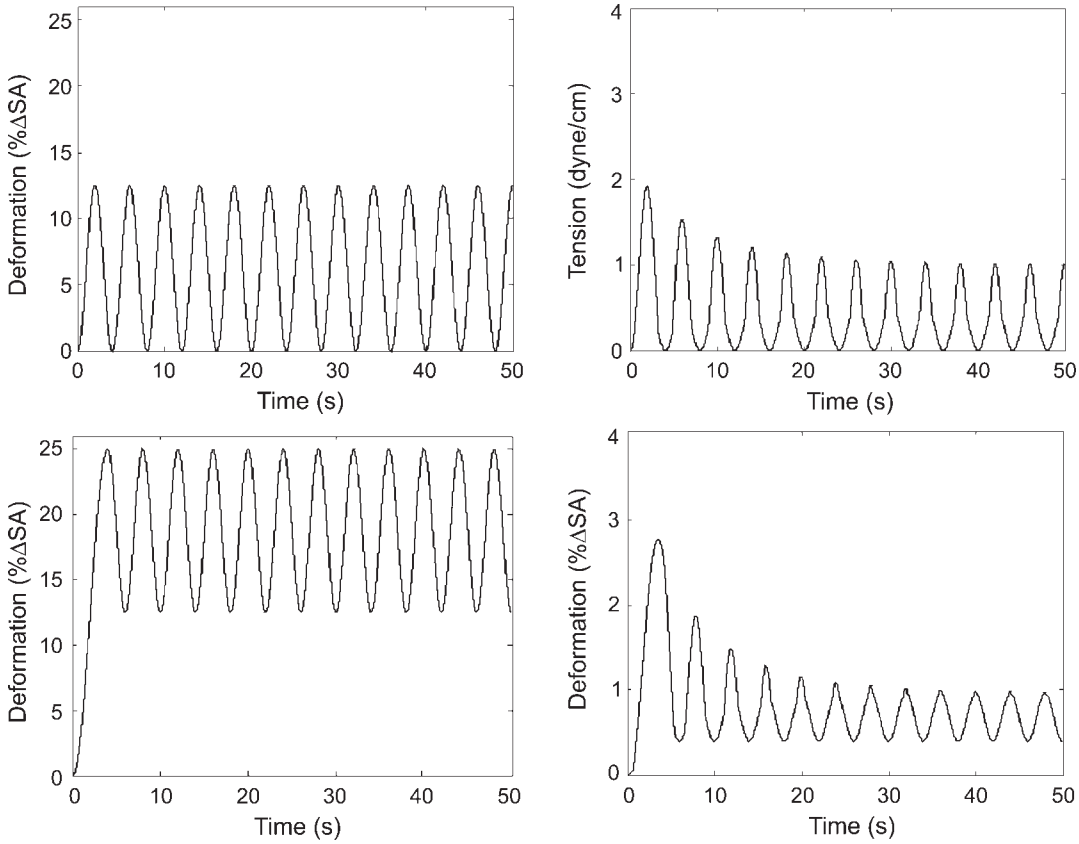

Fig. 9. Model tension output for a sampling of 2 additional deformation inputs. Deformation input waves and model-generated tension waves for 12% ΔSA cyclic stretch and 12–25% ΔSA cyclic stretch. For clarity, only the first few cycles are shown.

state (functional residual capacity) (53) and peak deformations of 12%, 25%, 37%, and 50% ΔSA. These peak deformations roughly correspond to ventilation of intact lungs to 70%, 90%, 100%, and >100% TLC, respectively (53), with no PEEP.

The second category includes ventilation with constant PEEP. PEEP is often used in mechanical ventilation to prevent derecruitment or collapse of alveoli when the lung is completely deflated; by maintaining a positive pressure at full expiration, the lungs remain open and partially inflated. PEEP values in clinical trials can range from 5 to 30 cmH_2O (3). In these studies, we have used three subcategories of PEEP. In the first subcategory, all waveforms had a maximum deformation of 25% ΔSA and a baseline deformation of 0%, 5%, 12%, 15%, or 20% ΔSA, corresponding roughly to 0, 5, 10, 12, and 15 cmH_2O PEEP. In the second PEEP subcategory, all deformation waves had an amplitude of 25% ΔSA with different PEEP and maximum deformation. The 15-cycle/min oscilla-

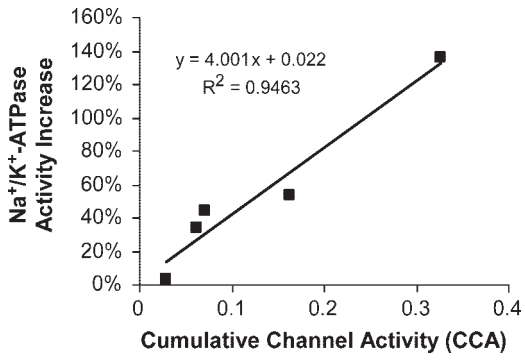

Fig. 10. Na^+-K^+-ATPase vs. cumulative stretch-activated channel activity (CCA). Increased Na^+-K^+-ATPase activity reported in previous studies (19) was plotted against a cumulative channel activity calculated by integrating SAC open probability of a stabilized tension cycle. From left to right, data points represent 25% ΔSA tonic stretch, 12% ΔSA cyclic stretch, 12–25% ΔSA cyclic stretch (PEEP), 25% ΔSA preconditioning, and 25% ΔSA cyclic stretch.

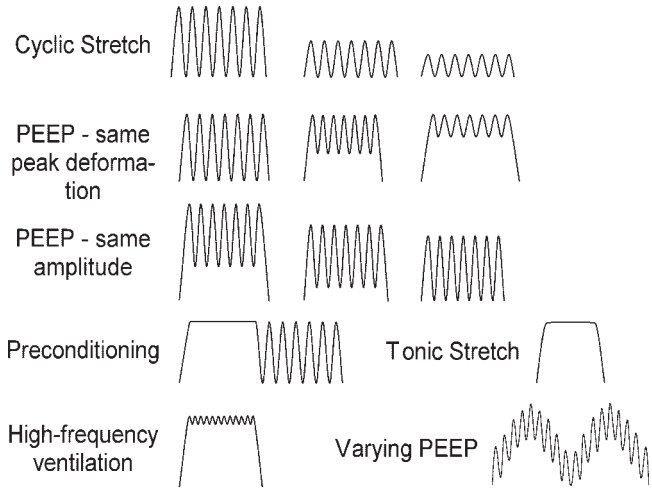

Fig. 11. Tested input wave forms. Shown here are examples of waveforms or sets of waveforms used as deformation inputs to the model.

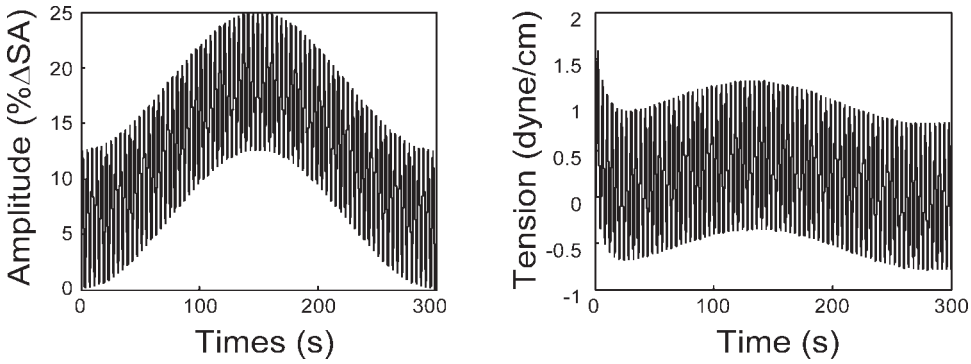

Fig. 12. Varying PEEP deformation input and tension output. The graph on the left depicts a 5-min varying PEEP wave with a fast frequency of 15 cycles/min and amplitude of 25% ΔSA superposed upon a shifting PEEP with a 0.2-cycle/min frequency and amplitude of 25% ΔSA. The graph on the right depicts tension generated by the model for the input on the left.

tions included 5–30%, 10–35%, and 20–45% ΔSA, corresponding to pressure ranges of 5–20, 8–29, and 15 to >40 cmH_2O. [In healthy lungs pressures greater than ≈30 cmH_2O generally correspond to inflation beyond 100% TLC; however, such pressures are not uncommon in critical care patients whose lungs are less compliant than normal, healthy lungs (53, 62).]

A third PEEP subcategory used sinusoidally varying PEEP at 0.2 cycles/min under a standard cyclic ventilation of 15 cycles/min (Fig. 12). One varying PEEP deformation wave had a PEEP range between 0 and 10 cmH_2O (0–12.5% ΔSA) and constant amplitude tidal volume wave of 12.5% ΔSA (peak deformation ranged between 12.5 and 25% ΔSA as PEEP varied). A second varying PEEP wave had a varying PEEP of 0–12 cmH_2O (0–10% ΔSA) under a 15-cycle/min deformation of 15% ΔSA (peak deformation ranged between 15 and 25% ΔSA as PEEP varied). Although shifting PEEP is not a standard clinical procedure, the idea was to test a ventilation pattern with low, noninjurious tidal volume but still substantially inflate the lungs on a 5-min cycle to prevent derecruitment or to recruit potential collapsed regions of the lung. In clinical ventilation an occasional deep breath or ventilator "sigh" is sometimes used for the same purpose, which benefits gas exchange and lung mechanics by recruiting additional, collapsed acini (1, 36). The varying PEEP ventilation proposed here aims to achieve the same lung recruitment volume but, by rising to it gradually, allow the alveolar epithelial cells to remodel their plasma membranes, decreasing plasma membrane tension and avoiding potential injury.

The third ventilation maneuvers category includes tonic deformation and HFV. As described in the introduction, in HFV the patient's lungs are maintained at a high PEEP and ventilated or "oscillated" at very low tidal volume at frequencies of 6–15 Hz. The lung essentially remains continuously inflated, and oxygenated air travels into the lungs through central channel in the airways while oxygen-poor air returns along the airway walls (38, 40, 46). Tonic deformation and HFV are grouped together because the large baseline deformation and comparatively small amplitude of HFV yield an input and an output very similar to tonic deformation.

Simulation Results

Cyclic ventilation (15 cycles/min). Standard cyclic ventilation was tested with peak deformations of 12%, 25%, 37%, and 50% ΔSA at a rate of 15 cycles/min. With increasing deformation, the peak tension of the steady-state response, T_{peak}, increased from 1.10 dyn/cm at 12% ΔSA to 3.35 dyn/cm with 50% ΔSA (Fig. 13). In the cyclic stretch category, only stretch at 50% ΔSA generated tensions reaching the plasma membrane lytic range of 3–4 dyn/cm (34) during steady-state deformation. However, considering the entire time course rather than just the steady-state response, stretch at 25% ΔSA and 37% ΔSA did generate lytic global maximum tensions, T_{gmax}, of 3.19 dyn/cm (Fig. 7*B*) and 4.72 dyn/cm, respectively, in their first cycle before steady state was reached. In this category, only cyclic stretch at 12% ΔSA maintained sublytic tensions throughout its time history, with T_{gmax} of 1.92 dyn/cm in the first cycle (Fig. 9*A*). For this group of ventilation forms, Na^+-K^+-ATPase activity (based on model-predicted CCA and its linear relationship to Na^+-K^+-ATPase activity, shown in Fig. 10) increased with a broader dynamic range from 25% increase at 12% ΔSA to a 327% increase at 50% ΔSA (Fig. 13). This broader range of Na^+-K^+-ATPase activity increase relative to T_{peak} results from the shape of the P_o function: while T_{peak} rose evenly with increasing deformation amplitude, P_o, and, in turn, Na^+-K^+-ATPase activity rose precipitously as tension approached or exceeded $T_{1/2}$ value of 1.4 dyn/cm.

PEEP ventilation. In the first subcategory of PEEP (waves with the same peak deformation of 25% ΔSA) steady-state T_{peak} was reduced as PEEP increased and tidal volumes decreased from 1.68 dyn/cm for 25% ΔSA cyclic stretch (0 PEEP) to 0.725 dyn/cm for 25% ΔSA PEEP, a tonic-stretch wave (Fig. 13). In contrast, Na^+-K^+-ATPase dropped steeply

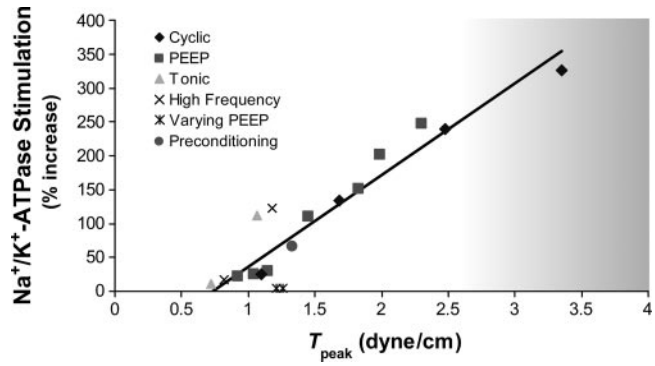

Fig. 13. Comparison of all ventilation maneuvers. From the perspective of stimulating Na^+-K^+-ATPase activity via plasma membrane tension and SAC activity while keeping tensions from becoming high enough to cause stress failure (shown as the shaded area to the right), high volume ventilation with PEEP and high frequency ventilation at 37% ΔSA yielded the highest return of Na^+-K^+-ATPase stimulation for tension risk (the distance of a point from the solid line representing an average group fit). Tonic stretch at 37% ΔSA also yielded a good result, but patients cannot be ventilated using tonic stretch.

as PEEP increased from 5% to 12% ΔSA baseline and tension fell below $T_{1/2}$ (Fig. 13). Thus, although increasing PEEP while decreasing tidal volume avoided lysis, Na^+-K^+-ATPase activity is predicted to decrease as well. Over the entire time course, T_{gmax}, always encountered in the first deformation cycle, was 3.19 dyn/cm for every wave with a peak deformation of 25% ΔSA, the same T_{gmax} for 25% ΔSA stretch. Because the first deformation wave is the same for all the PEEP waves in this category, the first tension waves are also alike.

In the second PEEP subcategory, deformations had constant amplitude (tidal volume), but peak deformation increased with greater PEEP. Expectably, T_{peak} rose as the entire deformation wave shifted upward to higher magnitudes. Even 20–45% ΔSA deformation, the greatest magnitude deformation in the category, maintained steady-state T_{peak} below the lytic tension range with a value 2.3 dyn/cm (Fig. 13). Here, Na^+-K^+-ATPase activity increased dynamically over the tested range (Fig. 13) due to a greater portion of the tension wave approaching or exceeding $T_{1/2}$. Of greatest concern in these simulations was T_{gmax} encountered during the first deformation from an undeformed state: 3.69 dyn/cm for 5–30% ΔSA, 4.68 dyn/cm for 10–35% ΔSA, and 6.21 dyn/cm for 10–45% ΔSA.

In the varying PEEP subcategory, the steady-state output had the same 5-min oscillatory period as the varying PEEP input. For this subcategory T_{peak} was defined as the highest peak tension over an entire 5-min steady-state wave. Similarly, CCA and thus Na^+-K^+-ATPase activity were calculated as an average over a 5-min period rather than over a single deformation wave. For the 15% ΔSA over 10% ΔSA varying PEEP simulation, T_{peak} was 1.21 dyn/cm, slightly higher than the 1.04 dyn/cm T_{peak} found for a similar 15–25% ΔSA constant PEEP simulation (Fig. 13). For the 12.5% ΔSA over 12.5% ΔSA PEEP simulation, T_{peak} was 1.26 dyn/cm, again slightly higher than the 1.15 dyn/cm T_{peak} found for a similar 12–25% ΔSA constant PEEP input. In contrast, average Na^+-K^+-ATPase activity was much lower for varying PEEP (<1% in both trials) due to long ranges of low tensions during the ebb of the PEEP wave. T_{gmax} values were safely sublytic: 1.72 dyn/cm for the first varying PEEP wave and 1.92 dyn/cm for the second wave, the same global peak tension found for a 12% ΔSA cyclic wave.

In sum, the PEEP waves generally produced lower steady-state T_{peak} than cyclic counterparts of the same peak deformation. However, constant amplitude (25% ΔSA) PEEP produced clearly higher Na^+-K^+-ATPase activity levels than constant deformation (25% ΔSA) and thus is likely to have a greater Na^+-K^+-ATPase activity "return" relative to the T_{peak} "risk." T_{gmax} for constant amplitude PEEP, however, was dangerously the same, suggesting that a slow initial climb to the high tidal volume should probably be used. The varying PEEP subcategory returned relatively low T_{peak} and low Na^+-K^+-ATPase activity, making it "safe" but not very effective in terms of stimulating SACs and ultimately the Na^+-K^+-ATPase edema clearance mechanism. These simulations concur with clinical use of moderate PEEP with reduced tidal volumes.

Tonic stretch and high frequency ventilation. Tonic stretch, analogous to a prolonged breath-hold, generally produced relatively low T_{peak} because relaxation occurred after the first deformation and tension was not perturbed afterward. As shown in Fig. 13, T_{peak} for 25% and 37% ΔSA tonic stretch remained well below the lytic threshold. We also note that a large contrast arises for Na^+-K^+-ATPase activity between 25% and 37% ΔSA tonic stretch because the 1.07-dyn/cm tonic tension of the latter is in the steep portion of the P_o curve, whereas the lower 0.73-dyn/cm tension of the former remains in the essentially flat portion of the curve, corresponding to almost no SAC opening.

Two HFV simulations were performed using low-amplitude waves with high PEEP, 24.5–25% ΔSA (25% ΔSA HFV) and 37–37.5% ΔSA (37% ΔSA HFV), at 10 Hz. The resultant tension and predicted SAC stimulation were similar to responses of similar magnitude 25% and 37% ΔSA tonic stretch. The extremely low amplitude kept T_{peak} at a low 0.82 dyn/cm for 25% ΔSA HFV and 1.18 dyn/cm for 37% ΔSA HFV. However, the extremely high frequency translates to high strain rate, which permitted very little relaxation within cycles and did, therefore, produce slightly higher tensions than those predicted for a pure tonic stretch (Fig. 13). Na^+-K^+-ATPase activity levels for HFV were also slightly higher than those for similar magnitude tonic stretch and showed the same contrast relative to the P_o curve (Fig. 13). For 25% ΔSA HFV, Na^+-K^+-ATPase activity increased only 11%, whereas for 37% ΔSA HFV, Na^+-K^+-ATPase jumped to 111%.

T_{gmax} values remained low in all tonic stretch and HFV because a slow 30-s rise was used for the first deformation. This slow rise was originally employed in tonic-stretch simulations to emulate experimental tonic-stretch protocols and was used in HFV as well to preserve the analogy between HFV and tonic ventilation.

DISCUSSION

Animal and in vitro studies have demonstrated that lung cells respond to stretch in ways both helpful and harmful to lung cell, whole lung, and whole organism health. They have also shown that the magnitude and frequency of cell deformation are critical determinants of how lung cells respond to stretch. The overall goal of this study was to develop a mathematical model linking stretch magnitude and frequency to tension in the plasma membrane, which we propose produces positive responses, such as Na^+-K^+-ATPase stimulation, and negative responses, such as plasma membrane rupture and cell death.

Traditionally, selection of ventilation volume and frequency has been based on providing adequate gas exchange and blood oxygenation, but as technical sophistication and understanding of pulmonary mechanics have increased, additional clinical objectives, including recruitment of collapsed lung regions, improving lung compliance, and preventing ventilator-induced injury, have been taken into consideration. Thus the medical community, including biomedical engineers, is posed with an optimization problem of maximizing ventilation benefits like gas exchange and oxygenation while minimizing injury responses, including increased epithelial permeability and alveolar edema, immune and inflammatory response, and cell death and high shear stresses associated with alveolar collapse and reopening. To truly optimize mechanical ventilation, one has to understand the synergistic and additive influences of the various components of a ventilation pattern, not just on the lungs as a whole but in the acini, lung cells, and, ultimately, even subcellular components. In this study, we have focused on the plasma membrane, which research has shown to be an impor-

tant factor in a cellular stretch response. Previously, we described how stimulation of SACs located in the plasma membrane improved Na^+-K^+-ATPase activity, a function that directly enhances edema clearance (19). On the other hand, Vlahakis et al. (58, 60) have shown that stretch, especially at high rates, can lead to alveolar epithelial cell plasma membrane stress failure. The goal of this research was to combine and extend limited experimental data regarding epithelial cell response to stretch by developing a predictive, mathematical model.

The results of these model simulations indicate that mechanical ventilation frequency, peak deformation, baseline or end-expiratory deformation, and ventilation history, as in the case of preconditioning, can play a critical role in plasma membrane tension, SAC opening, and Na^+-K^+-ATPase stimulation. They also demonstrate that waveforms can possibly be tailored to avoid lytic membrane tension while still achieving relatively high lung volumes required for adequate gas exchange and collapsed lung recruitment and maintaining a sublytic degree of membrane tension needed for maximal Na^+-K^+-ATPase stimulation.

Of clinical significance, constant PEEP ventilation, especially with constant amplitude and relatively high volume, appeared to produce the highest Na^+-K^+-ATPase stimulation relative to T_{peak} (Fig. 13). While T_{peak} and T_{gmax} remained sublytic, PEEP ventilation generated relatively high predictions of Na^+-K^+-ATPase stimulation relative to similar magnitude deformation without PEEP. This is because the baseline deformation forced a higher mean tension closer to $T_{1/2}$, maintaining a high probability of SAC opening and implying greater Na^+-K^+-ATPase stimulation. But, because relaxation had occurred over the static PEEP baseline, T_{peak} remained lower than in non-PEEP simulations. Three categories of PEEP ventilation were investigated: same peak deformation, same deformation amplitude, and slowly varying PEEP sinusoidally at 0.2 cycles/min. Slowly varying PEEP provided benefits similar to constant PEEP ventilation modes but to a lesser degree. T_{peak} with varying PEEP was slightly higher than similar amplitude constant PEEP ventilation (once every 5 min) because full relaxation was not able to occur as it could with constant PEEP. However, Na^+-K^+-ATPase stimulation was much lower in the former because tensions only rose every 5 min and the higher average tension of constant PEEP was not maintained. From the perspective of the whole lung, slowly varying PEEP might be valuable as a recruitment maneuver, but from the perspective of maintaining Na^+-K^+-ATPase while avoiding dangerous peak tension, constant PEEP appears to be a better option.

High frequency ventilation also appears to provide potential clinical benefit by increasing Na^+-K^+-ATPase activity with relatively low T_{peak} (Fig. 13). Because it almost mimics tonic stretch, tension remains nearly constant. At that level, Na^+-K^+-ATPase activity can be stimulated and lysis avoided by choosing high PEEP and smaller tidal volume. Therefore, despite other difficulties associated with high frequency ventilation, such as patient discomfort and recent doubts of the efficacy of HFV improving the risk of chronic lung disease (44), HFV does appear to be a useful strategy from the perspective of optimal Na^+-K^+-ATPase stimulation while avoiding plasma membrane injury.

In all simulated waveforms, plasma membrane tensions were high in the initial deformations before the tension response settled into a repeating steady-state response with lower peak magnitude. This high transient tension during the first cycles arises because no lipid insertion has occurred, leaving tension-generating elastic unfolding to accommodate the entire deformation. Later, after additional lipid material has inserted into the plasma membrane, the neutral area has increased, decreasing elastic deformations of the plasma membrane as seen by lower peak tension in the steady-state response. To avoid the risk of dangerously high plasma membrane tension and cell lysis in the clinical setting, it would be unwise to initiate ventilation in a lung that had been at rest for a prolonged period of time with the full desired tidal volume. Instead, one might start with a lower tidal volume and gradually increase volume of a period of the first 5–10 ventilation cycles to allow for an accumulation of additional plasma membrane before the full deformations of the target tidal volume are imposed.

The theoretical model developed here reveals some interesting phenomena about the response of the alveolar epithelial cell plasma membrane, SACs, and Na^+-K^+-ATPase to stretch and suggests potential strategies for improving epithelial cell survival and maximum, safe Na^+-K^+-ATPase stimulation. Nevertheless, there is certainly room for model refinement as better data and techniques for collecting better data become available. Most importantly, if it becomes possible to probe alveolar epithelial cell plasma membrane tension directly in real time during dynamic stretch, model predictions of membrane tension can be validated directly rather than through downstream increases in Na^+-K^+-ATPase activity. Fundamental assumptions of the model may also be refined as we develop a better understanding of how tension develops in the plasma membrane and how lipid insertion and resorption are stimulated at a molecular level. For now we have assumed that tension in an unfolding membrane increases linearly with the unfolding area strain. We have also assumed that lipid insertion rate is proportional to membrane tension. Although these are reasonable assumptions given the absence of better empirical knowledge, with the advent of better techniques for direct measurement of plasma membrane tension and dynamic lipid insertion, such assumptions might be refined. Inclusion of other mechanical factors, such as cytoskeletal influence, as they are better understood, could contribute to model improvement as well.

Also important is that the model predictions made in this communication are based on data for healthy lungs. Conversions from PEEP to TLC and from TLC to percent change in alveolar epithelial ΔSA were all based on normal lung models. In previous studies, Tschumperlin (53) modeled regional deformation in diseased or injured lungs by introducing a regional heterogeneity and found that large, injurious local alveolar epithelial deformations are likely even when using safe ventilation volumes and pressures. However, if the overall lung compliance is decreased by disease, actual epithelial deformations would be smaller for a given PEEP than predicted. To model diseased or injured lungs, the model input would have to be adjusted accordingly, as data become available.

In sum, this model is a valuable first step in demonstrating how plasma membrane unfolding and lipid insertion can work together to determine plasma membrane tension and Na^+-K^+-

ATPase stimulation in alveolar epithelial cells. The model provides a means of testing and comparing ventilation strategies from the perspective of plasma membrane tension and SAC stimulation, which are important elements in overall VILI. Using the model, we have identified constant PEEP ventilation, especially with constant amplitude and relatively high volume, and high frequency ventilation as leading mechanical ventilator maneuvers for stimulating moderate stretch-induced responses while preventing dangerously high plasma membrane tension. As shown in Fig. 13, these maneuvers predicted the highest Na^+-K^+-ATPase stimulation relative to peak membrane tension. It should also be noted that Na^+-K^+-ATPase stimulation is only one of many stretch-stimulated responses that clinicians might want to optimize, and optimal ventilation maneuvers may differ among desired responses. Ultimately, with the development of better methods for collecting more complete and more specific data for mechanically stretched alveolar epithelial cells and with better modeling of the cytoskeleton and cytoskeletal plasma membrane interactions, refined versions of this model and more sophisticated models for other responses can be built on the theoretical and empirical foundation developed here.

GRANTS

Support was provided by National Heart, Lung, and Blood Institute Grant R01-HL-57204.

REFERENCES

1. **Baldwin DN, Suki B, Pillow JJ, Roiha HL, Minocchieri S, and Frey U.** Effect of sighs on breathing memory and dynamics in healthy infants. *J Appl Physiol* 97: 1830–1839, 2004.
2. **Berrios JC and Hubmayr RD.** Deforming stress triggers endocytosis in alveolar epithelial cells (Abstract). *Am J Respir Crit Care Med* 167: A57, 2003.
3. **Brower RG, Lanken PN, MacIntyre N, Matthay MA, Morris A, Ancukiewicz M, Schoenfeld D, and Thompson BT.** Higher versus lower positive end-expiratory pressures in patients with the acute respiratory distress syndrome. *N Engl J Med* 351: 327–336, 2004.
4. **Chen CS and Ingber DE.** Tensegrity and mechanoregulation: from skeleton to cytoskeleton. *Osteoarthritis Cartilage* 7: 81–94, 1999.
5. **Dai J and Sheetz MP.** Cell membrane mechanics. *Methods Cell Biol* 55: 157–171, 1998.
6. **Dai J and Sheetz MP.** Regulation of endocytosis, exocytosis, and shape by membrane tension. *Cold Spring Harb Symp Quant Biol* 60: 567–571, 1995.
7. **Dai J, Sheetz MP, Wan X, and Morris CE.** Membrane tension in swelling and shrinking molluscan neurons. *J Neurosci* 18: 6681–6692, 1998.
8. **Dai J, Ting-Beall HP, and Sheetz MP.** The secretion-coupled endocytosis correlates with membrane tension changes. *J Gen Physiol* 110: 1–10, 1997.
9. **Dong C and Skalak R.** Leukocyte deformability: finite element modeling of large viscoelastic deformation. *J Theor Biol* 158: 173–193, 1992.
10. **Dong C, Skalak R, and Sung KL.** Cytoplasmic rheology of passive neutrophils. *Biorheology* 28: 557–567, 1991.
11. **Dong C, Skalak R, Sung KL, Schmid-Schonbein GW, and Chien S.** Passive deformation analysis of human leukocytes. *J Biomech Eng* 110: 27–36, 1988.
12. **Dos Santos CC and Slutsky AS.** Mechanisms of ventilator-induced lung injury: a perspective. Invited Review. *J Appl Physiol* 89: 1645–1655, 2000.
13. **Dreyfuss D and Saumon G.** Role of tidal volume, FRC, and end-inspiratory volume in the development of pulmonary edema following mechanical ventilation. *Am Rev Respir Dis* 148: 1194–1203, 1993.
14. **Dreyfuss D and Saumon G.** Ventilator-induced lung injury: lessons from experimental studies. *Am J Respir Crit Care Med* 157: 294–323, 1998.
15. **Dreyfuss D, Soler P, Basset G, and Saumon G.** High inflation pressure pulmonary edema. Respective effects of high airway pressure, high tidal volume, and positive end-expiratory pressure. *Am Rev Respir Dis* 137: 1159–1164, 1988.
16. **Fisher JL.** Mechanisms and means of Na^+-K^+-ATPase activation during alveolar epithelial stretch (Doctoral Thesis). Philadelphia, PA: University of Pennsylvania, 2004.
17. **Fisher JL, Levitan I, and Margulies SS.** Changes in alveolar epithelial cell plasma membrane surface area with static stretch. *2003 Summer Bioengineering Conference of the ASME Bioengineering Division*, Key Biscayne, Florida, 2003.
18. **Fisher JL, Levitan I, and Margulies SS.** Plasma membrane surface increases with tonic stretch of alveolar epithelial cells. *Am J Respir Cell Mol Biol* 31: 200–208, 2004.
19. **Fisher JL and Margulies SS.** Na+-K+-ATPase activity in alveolar epithelial cells increases with cyclic stretch. *Am J Physiol Lung Cell Mol Physiol* 283: L737–L746, 2002.
20. **Forgacs G.** On the possible role of cytoskeletal filamentous networks in intracellular signaling: an approach based on percolation. *J Cell Sci* 108: 2131–2143, 1995.
21. **Gajic O, Lee J, Doerr CH, Berrios JC, Myers JL, and Hubmayr RD.** Ventilator-induced cell wounding and repair in the intact lung. *Am J Respir Crit Care Med* 167: 1057–1063, 2003.
22. **Hamill OP and Martinac B.** Molecular basis of mechanotransduction in living cells. *Physiol Rev* 81: 685–740, 2001.
23. **Hao M and Maxfield FR.** Characterization of rapid membrane internalization and recycling. *J Biol Chem* 275: 15279–15286, 2000.
24. **Hase CC, Le Dain AC, and Martinac B.** Purification and functional reconstitution of the recombinant large mechanosensitive ion channel (MscL) of Escherichia coli. *J Biol Chem* 270: 18329–18334, 1995.
25. **Hochmuth FM, Shao JY, Dai J, and Sheetz MP.** Deformation and flow of membrane into tethers extracted from neuronal growth cones. *Biophys J* 70: 358–369, 1996.
26. **Hochmuth RM.** Cell biomechanics: a brief overview. *J Biomech Eng* 112: 233–234, 1990.
27. **Hochmuth RM.** Micropipette aspiration of living cells. *J Biomech* 33: 15–22, 2000.
28. **Ingber DE, Dike L, Hansen L, Karp S, Liley H, Maniotis A, McNamee H, Mooney D, Plopper G, Sims J, and et al.** Cellular tensegrity: exploring how mechanical changes in the cytoskeleton regulate cell growth, migration, and tissue pattern during morphogenesis. *Int Rev Cytol* 150: 173–224, 1994.
29. **Kloda A and Martinac B.** Structural and functional differences between two homologous mechanosensitive channels of *Methanococcus jannaschii*. *EMBO J* 20: 1888–1896, 2001.
30. **Le Dain AC, Saint N, Kloda A, Ghazi A, and Martinac B.** Mechanosensitive ion channels of the archaeon *Haloferax volcanii*. *J Biol Chem* 273: 12116–12119, 1998.
31. **Lewis SA and de Moura JL.** Incorporation of cytoplasmic vesicles into apical membrane of mammalian urinary bladder epithelium. *Nature* 297: 685–688, 1982.
32. **Markin VS and Martinac B.** Mechanosensitive ion channels as reporters of bilayer expansion. A theoretical model. *Biophys J* 60: 1120–1127, 1991.
33. **Mills LR and Morris CE.** Neuronal plasma membrane dynamics evoked by osmomechanical perturbations. *J Membr Biol* 166: 223–235, 1998.
34. **Morris CE and Homann U.** Cell surface area regulation and membrane tension. *J Membr Biol* 179: 79–102, 2001.
35. **Morris CE, Lesiuk H, and Mills LR.** How do neurons monitor their mechanical status? *Biol Bull* 192: 118–120, 1997.
36. **Mutch WA, Harms S, Ruth Graham M, Kowalski SE, Girling LG, and Lefevre GR.** Biologically variable or naturally noisy mechanical ventilation recruits atelectatic lung. *Am J Respir Crit Care Med* 162: 319–323, 2000.
37. **Needham D and Hochmuth RM.** A sensitive measure of surface stress in the resting neutrophil. *Biophys J* 61: 1664–1670, 1992.
38. **Priebe GP and Arnold JH.** High-frequency oscillatory ventilation in pediatric patients. *Respir Care Clin N Am* 7: 633–645, 2001.
39. **Raucher D and Sheetz MP.** Characteristics of a membrane reservoir buffering membrane tension. *Biophys J* 77: 1992–2002, 1999.
40. **Ritacca FV and Stewart TE.** Clinical review: high-frequency oscillatory ventilation in adults–a review of the literature and practical applications. *Crit Care* 7: 385–390, 2003.
41. **Sachs F and Morris CE.** Mechanosensitive ion channels in nonspecialized cells. *Rev Physiol Biochem Pharmacol* 132: 1–77, 1998.

42. **Satcher RL Jr and Dewey CF Jr.** Theoretical estimates of mechanical properties of the endothelial cell cytoskeleton. *Biophys J* 71: 109–118, 1996.
43. **Schneider SW.** Kiss and run mechanism in exocytosis. *J Membr Biol* 181: 67–76, 2000.
44. **Schreiber MD, Gin-Mestan K, Marks JD, Huo D, Lee G, and Srisuparp P.** Inhaled nitric oxide in premature infants with the respiratory distress syndrome. *N Engl J Med* 349: 2099–2107, 2003.
45. **Sheetz MP and Dai JW.** Modulation of membrane dynamics and cell motility by membrane tension. *Trends Cell Biol* 6: 85–89, 1996.
46. **Singh JM and Stewart TE.** High-frequency oscillatory ventilation in adults with acute respiratory distress syndrome. *Curr Opin Crit Care* 9: 28–32, 2003.
47. **Stamenovic D and Coughlin MF.** The role of prestress and architecture of the cytoskeleton and deformability of cytoskeletal filaments in mechanics of adherent cells: a quantitative analysis. *J Theor Biol* 201: 63–74, 1999.
48. **Stroetz RW, Vlahakis NE, Walters BJ, Schroeder MA, and Hubmayr RD.** Validation of a new live cell strain system: characterization of plasma membrane stress failure. *J Appl Physiol* 90: 2361–2370., 2001.
49. **Sukharev S.** Purification of the small mechanosensitive channel of Escherichia coli (MscS): the subunit structure, conduction, and gating characteristics in liposomes. *Biophys J* 83: 290–298, 2002.
50. **Tabarean IV and Morris CE.** Membrane stretch accelerates activation and slow inactivation in Shaker channels with S3–S4 linker deletions. *Biophys J* 82: 2982–2994, 2002.
51. **Tsai MA, Frank RS, and Waugh RE.** Passive mechanical behavior of human neutrophils: effect of cytochalasin B. *Biophys J* 66: 2166–2172, 1994.
52. **Tsai MA, Frank RS, and Waugh RE.** Passive mechanical behavior of human neutrophils: power-law fluid. *Biophys J* 65: 2078–2088, 1993.
53. **Tschumperlin DJ.** Deformation and injury of the alveolar epithelium (Doctoral Thesis). Philadelphia: University of Pennsylvania, 1998.
54. **Tschumperlin DJ and Margulies SS.** Alveolar epithelial surface area-volume relationship in isolated rat lungs. *J Appl Physiol* 86: 2026–2033, 1999.
55. **Tschumperlin DJ and Margulies SS.** Equibiaxial deformation-induced injury of alveolar epithelial cells in vitro. *Am J Physiol Lung Cell Mol Physiol* 275: L1173–L1183, 1998.
56. **Tschumperlin DJ, Oswari J, and Margulies SS.** Deformation-induced injury of alveolar epithelial cells. Effect of frequency, duration, and amplitude. *Am J Respir Crit Care Med* 162: 357–362, 2000.
57. **Vlahakis NE and Hubmayr RD.** Invited review: plasma membrane stress failure in alveolar epithelial cells. *J Appl Physiol* 89: 2490–2496; discussion 2497, 2000.
58. **Vlahakis NE and Hubmayr RD.** Response of alveolar cells to mechanical stress. *Curr Opin Crit Care* 9: 2–8, 2003.
59. **Vlahakis NE, Schroeder MA, Pagano RE, and Hubmayr RD.** Deformation-induced lipid trafficking in alveolar epithelial cells. *Am J Physiol Lung Cell Mol Physiol* 280: L938–L946, 2001.
60. **Vlahakis NE, Schroeder MA, Pagano RE, and Hubmayr RD.** Role of deformation-induced lipid trafficking in the prevention of plasma membrane stress failure. *Am J Respir Crit Care Med* 166: 1282–1289, 2002.
61. **Wan X, Harris JA, and Morris CE.** Responses of neurons to extreme osmomechanical stress. *J Membr Biol* 145: 21–31, 1995.
62. **West JB.** *Respiratory physiology: the essentials.* Baltimore, MD: Williams & Wilkins, 1990.
63. **Yeung A and Evans E.** Cortical shell-liquid core model for passive flow of liquid-like spherical cells into micropipets. *Biophys J* 56: 139–149, 1989.
64. **Zhelev DV, Needham D, and Hochmuth RM.** Role of the membrane cortex in neutrophil deformation in small pipets. *Biophys J* 67: 696–705, 1994.
65. **Zhu C, Bao G, and Wang N.** Cell mechanics: mechanical response, cell adhesion, and molecular deformation. *Annu Rev Biomed Eng* 2: 189–226, 2000.